Current Chemistry Letters 12 (2023) 557–566

Contents lists available at GrowingScience

Current Chemistry Letters

homepage: www.GrowingScience.com

A study on pseudo-potential effect, electronic structure, aquatic toxicity, and optical properties of perovskites solar cell of Cs_2NiCl_6, Cs_2NiBr_6, and Cs_2PtBr_6: Through DFT methods

Md. Hazrat Ali[a], Pritish Halder[a], Md. Siam Hossain[a], Julian Pretom Biswas[a], Sujan Sarker[a], Md. Kamruzzaman[a], Nurujjaman[a], Thamid[a], Md. Ishak Ali[a], Unesco Chakma[a,b] and Ajoy Kumer[b*]

[a]*Department Electrical and Electronic Engineering, European University of Bangladesh, Gabtoli, Dhaka, 1216, Bangladesh*
[b]*Laboratory of Computational Research for Drug Design and Material Science, Department of Chemistry, European University of Bangladesh, Dhaka, Bangladesh*

C H R O N I C L E

Article history:
Received December 20, 2022
Received in revised form
January 28, 2023
Accepted February 26, 2023
Available online
February 26, 2023

Keywords:
Band gap
Perovskite
Solar cells
Dielectric function and Aquatic toxicity

A B S T R A C T

The main impediment to practical application is the toxicity of lead ions in halide perovskite absorbing materials. Computing tools based on density functional theory (DFT) were used to predict the intrinsic properties of potential for double perovskites to be effective and suitable for optoelectronic applications, replacing the conventional lead halide perovskites with environmentally friendly elements. The Generalized Gradient Approximation (GGA) with Perdew-Burke-Ernzerhof (PBE) functional was used to screen homovalent alternatives for B and X-site ions in vacancy-ordered double perovskite Cs_2BX_6 (B=Pt, Ni, X= Cl, Br) for solar cell applications. Using the GGA with PBE functional, the band gap was calculated to be 1.411 eV, 0.482 eV, and 0.378 eV for the Cs_2PtBr_6, Cs_2NiCl_6, and Cs_2NiBr_6, respectively. The experimental band gap value of mother crystal's (Cs_2PtBr_6) was at 1.42 eV. Next, the DOS, PDOS and optical properties were computed using GGA with PBE functional. Then, the local density approximation (LDA) with Ceperley and Alder with Perdew and Zunger (CA-PZ) was executed to compare the GGA with PBE for electronic band structure. In addition, the OTFG ultra soft, OTFG norm conserving, ultra soft and norm conserving methods of pseudopotential were used for both GGA with PBE and LDA with CA-PZ to make and ensure the right or accurate DFT functional for those crystals. At last, the optical properties and their toxicity have been evaluated for their rational design of potential double perovskite materials with improved optoelectronic properties.

© 2023 by the authors; licensee Growing Science, Canada.

1. Introduction

Due to their superb optoelectronic and photovoltaic properties, all-inorganic metal-halide perovskite nanocrystals (NCs) have received a lot of attention in solar cells, [1] light-emitting diodes (LED), [2] temperature sensors, [3] lasers, [4] and photodetectors [5]. These characteristics consist of a large absorption cross-section, a long diffusion distance, and high carrier mobility [6]. Perovskites perform very differently depending on their composition. As a result, numerous efforts have been made in recent years to design and prepare various types of all-inorganic halide perovskites. Most lead-containing perovskites currently lose structural integrity when exposed to moisture, oxygen, or light [7]. Typical lead-based hybrid perovskites utilize the $APbX_3$ structure, in which A site is an organic or inorganic cation (such as methyl ammonium, Cs+), and X is a halide (mainly I or Br) [8]. Their exceptional optoelectronic characteristics, including their high optical absorption coefficient, carrier diffusion lengths up to 1 mm^9 low trap density in the range of 1016–1017 cm^3, shallow defect states, and low excited binding energy, are the reason behind their high performances [10]. Perovskite-based nanomaterials use in

* Corresponding author.
E-mail address kumarajoy.cu@gmail.com (A. Kumar)

© 2023 by the authors; licensee Growing Science, Canada
doi: 10.5267/j.ccl.2023.2.007

photoelectron chemistry (PEC) and photocatalysis, particularly in the aqueous phase, has been constrained by these stability issues [11]. Consequently, Lead is one of the three major heavy metal contaminants, as well as a heavy metal element, that poses serious risks to humans and the environment [12-13]. The lead can seriously endanger health even with minor exposure, leading to issues like impaired brain development, renal failure, and nerve damage [14]. As a result, it also impedes large-scale production and commercialization of lead halide perovskite although applied sciences are very important in different fields and this concept was reported before in a lot of papers [15-21].To overcome these constraints, researchers are focusing on replacing Pb with non-toxic metals, and the development of stable alternatives is urgently needed. The Pb^{2+} can be easily replaced with less harmful group IV metal ions like Sn^{2+} or Ge^{2+} due to their similar electronic structure to Pb in order to produce lead free ternary $A_1M_2{+}X_3$ halide perovskites [22]. Optoelectronic devices perform poorly when using Sn^{2+}/Ge^{2+} halide perovskites because they are incredibly unstable in the air and easily oxidize to Sn^{4+}/Ge^{4+} [23]. Lead-free quaternary $A_2M^{+}M^{3+}X_6$ double perovskites (A = Cs^{+}; M^{+} = Cu^{+}, Ag^{+}, Na^{+}; M^{3+} = Bi^{3+}, Sb^{3+}, In^{3+}; X = Cl^{-}, Br^{-}, I^{-}) are another option which have been prepared by replacing two Pb^{2+} cations with a pair of nontoxic heterovalent metal ions ($2Pb^{2+} \rightarrow M^{+} + M^{3+}$) [24].

According to the perovskite frameworks, a suitable and direct band gap is a crucial requirement for photovoltaic (PV) systems used in light-absorbing applications. For M+/M3+ sites, the most commonly reported double perovskite combination is Ag and Bi or in elements. In general, these perovskites have large bandgaps ($Cs_2AgBiCl_6$ for 2.77 eV, [25] $Cs_2AgBiBr_6$ for 2.2 eV, [26] and $Cs_2AgInCl_6$ for 3.23 eV, [27]), and they only absorb light in the ultraviolet region, [28] which makes them unsuitable for the vast number of photovoltaic applications [29]. In order to date, bandgap engineering techniques such as metal alloying, [30] anion-exchange reactions, [31] and metal ion doping have all been tried in an effort to reduce the bandgap of double perovskite.

According to the formula of $A_2M_4{+}X_6$, it is a general formula that can be used to maintain charge neutrality by using one tetravalent metal cation and one vacancy site [32]. Cai et al. reported that they calculated the electronic structure and energy stability of A_2BX_6 halide compounds (A= Rb and Cs; B= Sn, Pd, and Pt; and X= Cl, Br, and I) using density functional theory (DFT) and hybrid (HSE06) functional theory [33]. A few promising candidate materials, mainly based on theoretical predictions, have been successfully synthesized such as Cs_2SnI_6 and Cs_2PdBr_6 [34-35]. Therefore, it is still today very important to investigate stable Pb-free halide perovskites with a small band gap.

The most advanced hierarchical calculation method based on first principles is used for primary screening throughout the DFT framework [36]. There are many DFT functional (basis set) for calculating the electronic properties, optical properties and structural geometry. In general, the Perdew–Burke–Ernzerhof (PBE), revised Perdew–Burke– Ernzerhof (RPBE), Perdew–Wang (PW91), Wu–Cohen (WC), and Perdew–Burke–Ernzerhof for solids (PBEsol) nonlocal functionals of the generalized gradient approximation (GGA) are very common basis sets for calculation [37-41]. The geometric structure of the perovskites, bandgaps of the optimized perovskites, and optical properties were calculated using the GGA with PBE method which is the most accurate method for the crystallographic properties. We used a single process to prescreen the materials with solar cell application potential. This study also revealed that the first vacancy-ordered perovskite material, the Cs_2NiCl_6 and Cs_2NiBr_6 had a narrow bandgap (0.482 eV and 0.378 eV), excellent photoelectric performance, and highly stable air-tolerant properties, with high absorption value in the visible range. The dielectric constant and absorption coefficient of Cs_2PtBr_6 were lower than those of other perovskites. This research establishes a solid theoretical foundation for understanding the structural and electronic properties of these compounds.

2. Results and discussion

2.1 Structural properties

According to our calculations, the vacancy-ordered C_2BX_6 (B=Pt, Ni, and X=Cl, Br) have a face-centered cubic structure with the space group Fm3m (International Number 225). The geometrical arrangement and atomic positions of C_2BX_6, which is an example of an ABX_3 perovskite with a [BX_6] cluster. The empty spaces between [BX_6] octahedra are filled with A-site atoms. The A_2BX_6 structure consists of six [BX_6] octahedra that are isolated from one another and form a 12-fold coordination environment for discrete X anions. The [BX_6] octahedra form a cubic environment when placed at the corners and face center positions. The A-site atoms are located at the 8c Wyckof site and in the fractional coordinates (1/4, 1/4, 1/4), the B-site cations are at the 4a Wyckof site and in the fractional coordinates (0, 0, 0), and the X-anions are at the 24e Wyckof site. The variable x is near 0.2.

After optimizing their crystal structures, which were listed in table 1 as the fundamental structural unit, using the PBE methods and attempting to maintain their similar parameters to appear at a comparative study at a point, the values of the lattice parameters for Cs_2PtBr_6, Cs_2NiCl_6, and Cs_2NiBr_6 were determined from the Materials Studio. Furthermore, it is important to point out that the structural optimization simulated by GGA with PBE in **Fig. 1(a)-(c)** calculated the electronic structure and optical properties of a crystal containing heavy metal atoms, which was thought to be the standard function of DFT.

Table 1. Structural calculation by four methods of Cs_2PtBr_6, $Cs_2NiCl_6$and Cs_2NiBr_6

Compounds	a	b	C	α	β	γ	Crystal type	Space group	Density
Cs_2PtBr_6	11.05Å	11.05Å	11.05Å	90.000°	90.000°	90.000°	Cubic	$Fm\bar{3}m$	4.63g·cm^{-3}
Cs_2NiCl_6	11.05Å	11.05Å	11.05Å	90.000°	90.000°	90.000°	Cubic	$Fm\bar{3}m$	4.63g·cm^{-3}
Cs_2NiBr_6	11.05Å	11.05Å	11.05Å	90.000°	90.000°	90.000°	Cubic	$Fm\bar{3}m$	4.63g·cm^{-3}

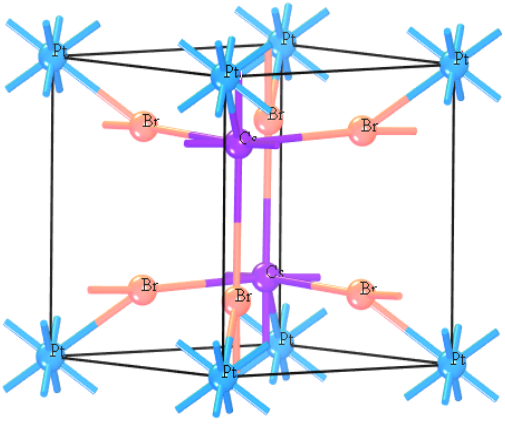

Fig. 1. a) Optimized structure of Cs_2PtBr_6

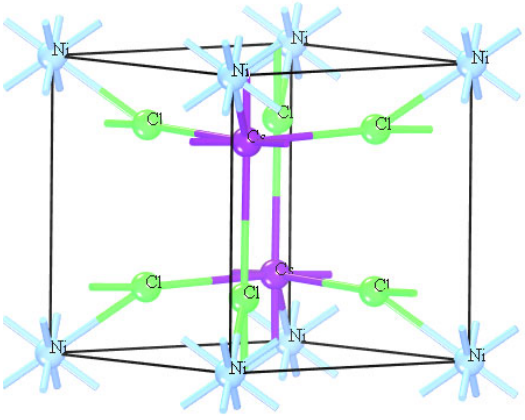

Fig. 1. b) Optimized structure of Cs_2NiCl_6

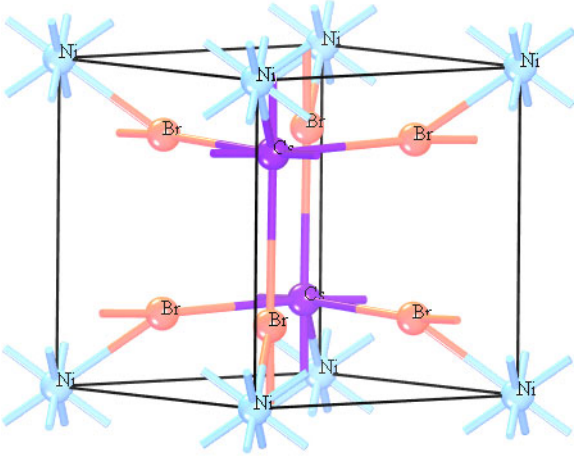

Fig. 1. c) Optimized structure of Cs_2NiBr_6

2.2 Electronics structure

Table 2. Band gap with respect to various functional of crystals

Crystal	Band gap	references
Cs_2PtBr_6 (Mother Crystal)	1.411 eV	1.420 eV [42]
Cs_2NiCl_6	0.482 eV	New predicted
Cs_2NiBr_6	0.378 eV	New predicted

The bandgap of these perovskite materials is one of their key properties. The DFT method was used to determine the bandgaps of these three perovskites at the PBE levels, and the results were used as a pre-screening benchmark. However, The PBE functional typically overestimates the bandgaps of periodic systems. The bandgap was across at 1.411 eV, 0.482 eV and 0.378 eV for Cs_2PtBr_6, Cs_2NiCl_6 and Cs_2NiBr_6 crystals, respectively, through the GGA with PBE functional. In accordance with the results of theoretical calculations, perovskites containing Cs_2PtBr_6 have bandgaps that are too wide for single-junction perovskite solar cells, but Cs_2NiCl_6 and Cs_2NiBr_6 have incredibly narrow bandgaps and obtain semiconductor properties as shown in **Fig. 2(a)-2(b)**. It can be assumed that the investigated perovskites, composed of double perovskites based on cesium, cannot perform a promising single solar cell. It should be noted that the bandgap reduces as the B-site cations in Ni change, and the transition from chloride to bromide gradually narrows the bandgap; this will be important for the bandgap regulation engineering of perovskites. Moreover, the Fermi level is at 0.0 eV, and the conduction and valence bands are on opposite sides of the Fermi energy level, with the conduction band on the upper side and the valence band on the lower side. The minimum conduction band (MCB) and maximum valence band (MVB) are both found at point G for Cs_2PtBr_6, Cs_2NiCl_6 and Cs_2NiBr_6 crystals, respectively. Table 2 explains the Cs_2PtBr_6 experimental

bandgaps from other literature and the theoretical results also demonstrate the bandgap of Cs_2PtBr_6, Cs_2NiCl_6 and Cs_2NiBr_6 crystals.

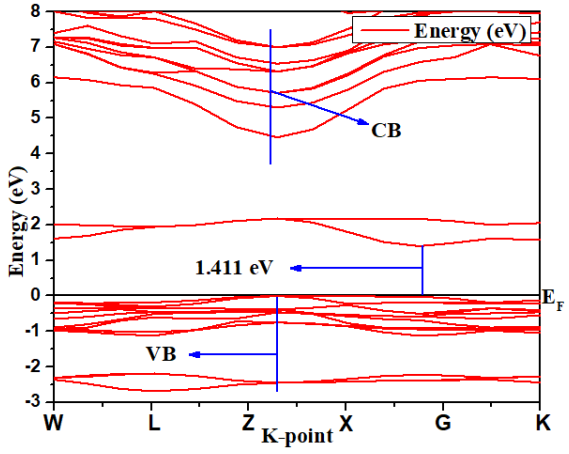

Fig. 2. a) Band structure for Cs_2PtBr_6

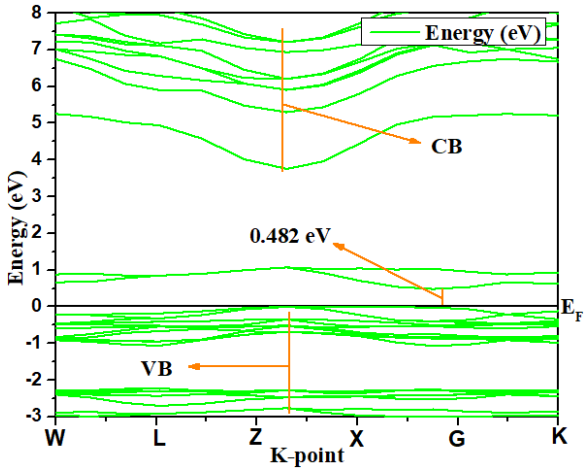

Fig. 2. b) Band structure for Cs_2NiCl_6

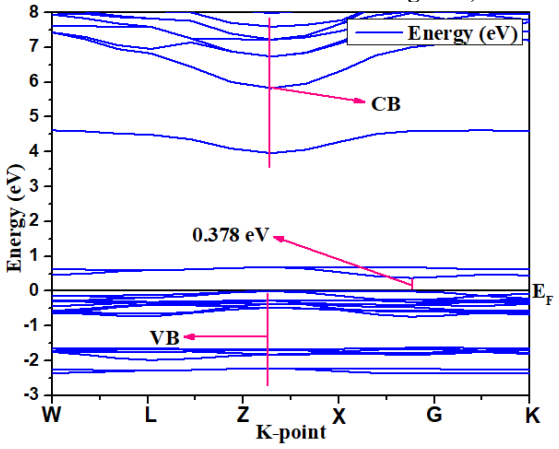

Fig. 2. c) Band structure for Cs_2NiBr_6

In case of the OTFG ultra soft, OTFG norm conserving, ultra-soft and norm conserving method of pseudopotential, the Norm conserving is the most accurate value among other accounting of experimental value (1.420 eV) by GGA with PBE listed in Table 3.

Table 3. Band gap by four pseudo-potential methods in eV

Crystals	OTFG Ultra soft		OTFG norm conserving		Ultra soft		Norm conserving	
	GGA with PBE	LDA with CA-PZ	GGA with PBE	LDA with CA-PZ	GGA with PBE	LDA with CA-PZ	GGA with PBE	LDA with CA-PZ
Cs_2PtBr_6 (Ref Crystal)	1.390	1.268	1.394	1.270	1.402	1.262	1.411	1.379
Cs_2NiCl_6	0.329	0.254	0.335	0.262	0.342	0.285	0.482	0.325
Cs_2NiBr_6	0.262	0.240	0.275	0.255	0.295	0.271	0.378	0.285

2.3 The total density of states (TDOS) and partial density of states (PDOS)

The DOS was used to investigate the electronic properties of Cs_2PtBr_6, Cs_2NiCl_6 and Cs_2NiBr_6 compounds. **Fig. 3(a)** to **3(d)** displays the total density of states (TDOS) and partial density of states (PDOS) plots. The fact that the TDOS of VB does not pass through the Fermi level indicates that all the materials are semiconducting. The understanding of orbital properties helps to explain how each atom's electronic contribution to the stabilized structure. **Fig. 3(a)** and **Fig. 3(b),** which show that the Cs orbitals of these four materials are located far from the Fermi level, suggest that the Cs has little influence on the band edge states for Cs_2PtBr_6. Additionally, the Pt -d and Br -p orbitals both contribute to the formation of this conduction band edge (CBE). The Cs orbitals of Cs_2NiCl_6 are shown in **Fig. 3(c)** to be located far in the VB (-2.5 eV),

contributing little to the VB and CB close to the Fermi level. The p orbital of Cl contributes significantly to a valence band edge (VBE), and as carriers gain energy, electrons move from the VB to the CB. For Cs_2NiBr_6, the Br-p orbitals and Cs orbitals both contribute significantly to the VBE, with Cs also present deep in the VB and CB (7 eV) as shown in **Fig. 3(d).** The Br-p orbitals dominate the CB region near the Fermi level, while Ni-d orbitals dominate the core region of CB.

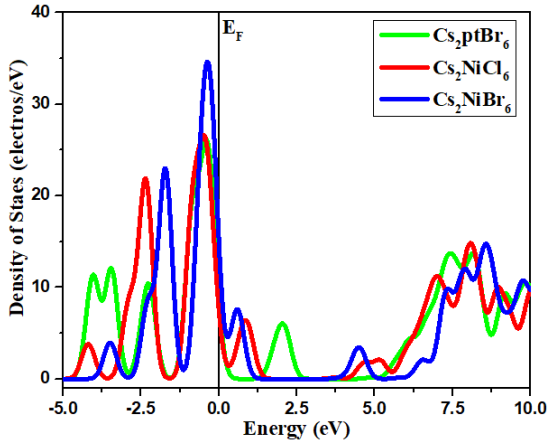

Fig. 3. a) Total DOS for Cs_2PtBr_6, Cs_2NiCl_6 and Cs_2NiBr_6

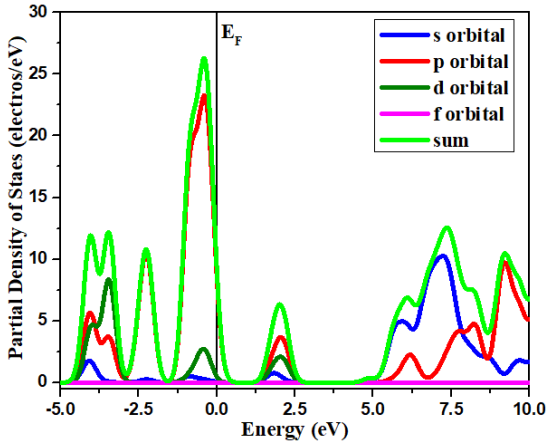

Fig. 3. b) Partial Density of States for Cs_2PtBr_6

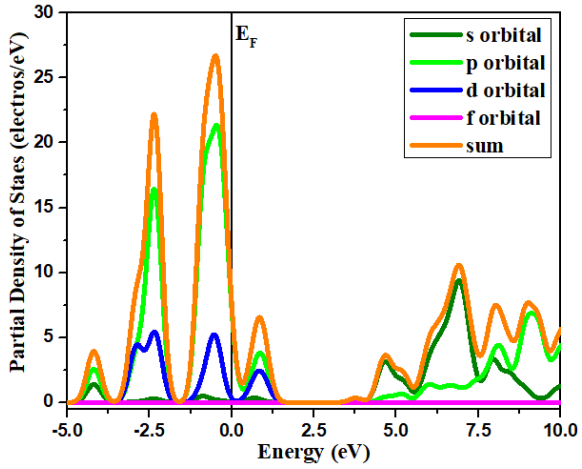

Fig. 3. c) Partial Density of States for Cs_2NiCl_6

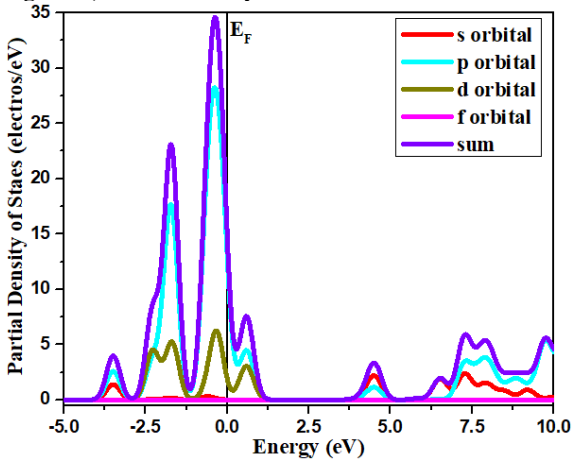

Fig. 3. d) Partial Density of States for Cs_2NiCl_6

2.4 Optical Properties

Solid-state optical properties are highly sensitive to bandgap nature, electron recombination rate, and electron-photon interaction. It is highly essential to describe the optical properties of any material because the dielectric constant is used to calculate various optical parameters, including refractive index, absorption, conductivity, reflectivity, and loss function. According to the Kramers-Kronig equations can be used to compute the frequency-dependent complex dielectric function [43]:

$$\varepsilon(\omega) = \varepsilon_1(\omega) + \varepsilon_2(\omega)$$

Dielectric function has been calculated using PBE function. The ω represents the angular frequency of electromagnetic radiations.

The angular frequency of electromagnetic radiation is represented by ω. The polarization and dispersion of the light that is impinging have been defined by the $\varepsilon_1(\omega)$ (real part of the dielectric constant), while the $\varepsilon_2(\omega)$ (imaginary part of the dielectric constant) depicts how light is absorbed by materials. **Fig. 4** shows the calculated $\varepsilon_1(\omega)$ and $\varepsilon_2(\omega)$ of Cs_2BX_6 (B=Pt and Ni; X=Cl and Br) against incident energy. The $\varepsilon_1(0)$ (static dielectric constant) can be calculated from the low energy limit of $\varepsilon_1(\omega)$, which begins at 4.40, 6.83, and 8.20 with the energy of the incident electromagnetic waves for Cs_2PtBr_6, Cs_2NiCl_6, and Cs_2NiBr_6 crystals, respectively.

In the low energy region at 0.5 eV to 3.0 eV, it also seems that there are three resonance $\varepsilon_1(\omega)$ peaks for Cs_2NiCl_6, and Cs_2NiBr_6 crystals. These peaks represent the maximum light dispersion and specific light energy at plane polarization[58]. Furthermore, the value of $\varepsilon_1(\omega)$ is positive in the lower energy region (0-5 eV) and ensures the predominant semiconducting

behavior. The studied comparisons show good dielectric constants suitable for optical applications in the visible spectrum. Furthermore, the calculated dielectric functions of Cs_2NiCl_6 and Cs_2NiBr_6 crystals are always greater than the mother crystal (Cs_2PtBr_6). The larger the dielectric constant, the stronger the dielectric's ability to bind the electron and the less likely the electron is to be polarized [44].

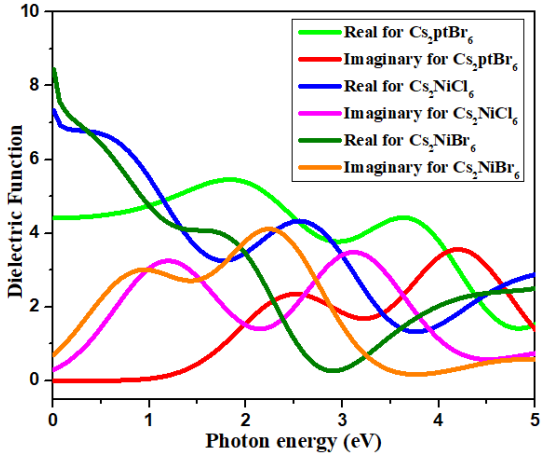

Fig. 4. Dielectric Function

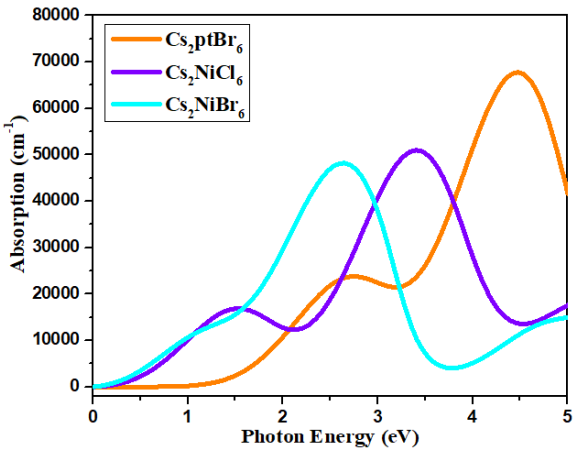

Fig. 5. Absorption

Furthermore the application of photoelectric or solar cells, the absorption coefficients α(ω) are investigated from ε1(ω) and ε2(ω) through the following equation [45]:

$$\alpha(\omega) = \sqrt{2}\omega\left\{\sqrt{\varepsilon\frac{2}{1}(\omega) + \varepsilon\frac{2}{2}(\omega)} - \varepsilon_1(\omega)\right\}^{\frac{1}{2}}$$

Fig. 4 illustrates the calculated values of the α(ω), which express how much light energy is absorbed by the semiconductor. The $\varepsilon_2(\omega)$ also represents the material's light absorption capacity. When we compare the $\varepsilon_2(\omega)$ and α(ω) curves, we can observe a similar trend; however, some peaks have been displaced as a result of the various theoretical approximation methods that were applied to the computation of these two curves. Several absorption peaks in the energy range of more than 1 eV are present in all of the materials under investigation, indicating that they are ideal for optoelectronic devices that operate in both the ultraviolet and visible light spectrums. Compared to the Cs_2PtBr_6 crystal, the peak absorption values of the Cs_2NiCl_6 and Cs_2NiBr_6 crystals are higher, ranging from 50000 cm1 to 58000 cm1 in the visible spectrum (1.4- 3.5 eV). Moreover Cs_2GeBr_6 has the lowest absorption peak at 2.5 eV, which is low to photoelectric performance in the visible range compared with the absorption curve of other compounds.

2.5 Aquatic toxicity

The presence of the hazardous element Pb, whose use is severely restricted and regulated in many countries due to its harmful effects on human health and the environment. The toxicity issue is primarily addressed by suggesting new substituting materials for lead, even though their instability is a real, serious problem that needs to be (and has been partially) mitigated. The study of chemical and other anthropological and natural materials' effects on aquatic organisms, as well as how activity on these organisms affects communities and ecosystems through individual organisms, is known as aquatic toxicity. The toxicity of used materials is an important consideration before use authorization in cases involving the safety of aquatic organisms. To generate a toxicity profile for the predicted bio-inorganic crystals, computational tools, such as AMES toxicity, honey bees, rats, and fish, carcinogenicity, and inhibition have all been implemented.

There is positive response for Cs_2NiCl_6 to AMES toxicity except but slightly danger for other two crystals. Secondly, all crystals have no barrier of nature by any organism, so there is no chance of entering living cells to cause damage or adverse effects for other diseases; even after entering the living cell, the carcinogenic effect is almost non-existent. On the other hand, table 3 demonstrates that these crystals' solubility is close to that of organic compounds, which is close to -3.0 or lower. The novel response from these crystals is explained by the effect of halogen atoms, where the solubility changes due to changes in the electronegative atoms in a way that is related to size rather than electronegativity. It grows larger as the size is increased, and this is similar to other parameters. Finally, these crystals are eco-friendly materials. The most important fact is noted that they are not ready biodegradable materials so that there is no scope for entering the human body or environment.

Table 4. Aquatic and non aquatic toxicity

	AMES toxicity	Inhibition	Carcinogenicity	Water solubility, Log S	Acute Oral Toxicity, kg/mol	Oral Rat Acute Toxicity (LD50) (mol/kg)	Honey Bee Toxicity	Fish Toxicity pLC50 mg/L	T.Pyriformis toxicity (log µg/L)	Biodegradation
Cs_2PtBr_6	Yes	No	No	-3.267	0.427	2.746	High	1.3334(Low)	1.1491 (High)	Not ready biodegradable
Cs_2NiCl_6	Slightly Danger	No	No	-3.317	0.473	2.840	High	1.4321 (Low)	0.831 (Low)	Not ready biodegradable
Cs_2NiBr_6	Slightly Danger	No	No	-3.267	0.427	2.746	High	1.3334 (Low)	0.829 (Low)	Not ready biodegradable

3. Conclusion

The creation and use of solar cells are significant technologies for renewable energy, particularly in light of the expanding demand for clean energy and the focus on environmental protection technology. However, due to its toxicity, the lead-based perovskite cannot be widely accepted for sustainable uses. Environmentally friendly materials are desperately needed to overcome the main application bottleneck. The development of environmentally friendly materials may be accelerated through the finding of promising alternatives to lead-containing perovskite through the theoretical prediction results of perovskite properties covering various elements. The structural, electronic, and optical properties of Cs_2BX_6 compounds were calculated using first-principles PBE calculations with two combinations of B = Pt and Ni cations, X =Cl and Br halogen ion. For single-junction perovskite solar cells, the calculated bandgap of perovskites containing Cs_2PtBr_6 is too large, but structures combining Cs_2NiCl_6 and Cs_2NiBr_6 also gave extremely narrow bandgaps. Theoretical results also showed that every perovskite under investigation follows the typical pattern of replacing halogen (Cl > Br) to change the bandgap. It serves as a guide for the application of Cs-based halide double perovskite bandgap engineering. The bandgaps of the selected perovskites are predicted to range from 0.482, 0.378, and 1.411 eV for Cs_2NiCl_6, Cs_2NiBr_6, and Cs_2PtBr_6, respectively. They are suitable for optoelectronic devices under visible and ultraviolet light because they have multiple absorption peaks in the energy range at 1 eV. The DFT study can provide theoretical guidance and support the rational design of high-performance double perovskites for optoelectronic applications of solar cells.

Acknowledgments

The authors would like to thanks, Debashis Howlader, Lab officer, Department of Electrical and Electronic Engineering, EUB, Dhaka, Bangladesh.

Disclosure statement: No potential conflict of interest was reported by the author(s)

4. Computational methods

According to the CASTEP code [46-48] implementation of DFT [49-50], the first-principle calculations were carried out using the plane-wave basis and pseudopotential methods. We used to calculate the electronic structure and optical properties through the generalized gradient approximations (GGA) [51-57] with Perdew-BurkeErnzerhof (PBE) [58-67] functional. Each exchange-correlation (XC) functional was calculated using a 3×7×5 Monkhorst-Pack grid and two different kinetic-energy cutoffs, 500 eV at norm conserving. The tolerance for self-consistent fields (SCF) was 1.010^{-6} (eV/atom). The maximum ionic Hellmann-Feynman force, maximum ionic displacement tolerance, and total energy tolerance were 2.0×10^{-6} (eV/atom), 0.006 (eV/Å) and 2.0×10^{-6} (Å), respectively. A dense mesh of uniformly distributed k-points is required for the optical spectra calculations; thus, the Brillouin zone integration was performed using a 3×7×5 grid of Monkhorst-Pack points. Following that, optical features such as dielectric function and absorption were optimized and simulated using the GGA with PBE functional, with cut-offs of 508 eV at norm conserving pseudo potentials, grid 3×7×5, and minimum energy. Following simulation, the optical properties of Cs_2PtBr_6, Cs_2NiCl_6, and Cs_2NiBr_6 were calculated using the materials studio analysis option.

References

1 Xiang W., Tress W., (**2019**) Review on recent progress of all-inorganic metal halide perovskites and solar cells. *Adv. Mater.,* 31 (44), 1902851.

2 Chang H. D., Das D., Varde P. V., Pecht M. (**2012**) Light emitting diodes reliability review. *Microelectron. Reliab.,* 52 (5), 762-782.

3 Zhang S., Yu F., (**2011**) Piezoelectric materials for high temperature sensors. *J. Am. Ceram. Soc.,* 94 (10), 3153-3170.

4 Samuel I. D. W., Yang Y., Wang Y., Turnbull G. A., (**2007**) Organic semiconductor lasers. *Chem. Rev.,* 107 (4), 1272-1295.

5 Lin C. H., Liu W. C., (**2010**) Metal-insulator-semiconductor photodetectors. *Sensors.,* 10 (10), 8797-8826.

6 Gamliel S., Lioz E., (**2014**) Organo-metal perovskite based solar cells: Sensitized versus planar architecture. *RSC Adv.,* 4 (55), 29012-29021.

7 Djurišić A. B., Liu F.Z., Tam W. H., Wong K. M., Ng A., Surya C., Chen W., He Z. B., (**2017**) Perovskite solar cells-an overview of critical issues. *Prog. Quantum.,* 53, 1-37.

8 Ding D., Henan L., Jieni L., Zibo L., Lui L., Tian B. B., Su C., Chen F., Shi Y., (**2019**) Effect of mechanical forces on thermal stability reinforcement for lead based perovskite materials. *J. Mater. Chem.,* 7 (2), 540-548.

9 Li W. G., Rao S. H., Chen X. B., Wang D. X., Kuang B. D.,(**2017**) A formamidinium–methylammonium lead iodide perovskite single crystal exhibiting exceptional optoelectronic properties and long-term stability. *J. Mater. Chem.,* 5 (36), 19431-19438.

10 Harikesh C. P., Wu B., Ghosh B., Jhon A. B., Lie S., Thirumal K., Wong H. L., Sum C. T., Mhaisalkar S. Mathews N., (2018) Nripan Metal cation transmutation enabled doping and switchable photovoltaic effect in lead free perovskite with extended carrier lifetimes, *Adv. Mater.*, 1802080 (1-8).

11 Armenise V., Silvia C., Francesco F., Andrea L., (**2021**) Lead-free metal halide perovskites for hydrogen evolution from aqueous solutions. *J. Nanomater.,* 11 (2), 433.

12 Ali H., Khan E., Ilahi I., (**2019**) Environmental chemistry and ecotoxicology of hazardous heavy metals: Environmental persistence, toxicity, and bioaccumulation. *J. Chem.,* 2019.

13 Alengebawy A., Abdelkhalek T. S., Qureshi R. S., Wong Q. M. (**2021**) Heavy metals and pesticides toxicity in agricultural soil and plants: Ecological risks and human health implications. *Toxics,* 9 (3), 42.

14 Steffan J. J., Brevik E. C., Burgess C. L., Cerdà A., (**2018**) The effect of soil on human health: An overview. *Eur. J. Soil Sci.,* 69 (1), 159-171.

15 Saber F. A., Sayed M., Tolba S. M., S., El-Deana K. M. A., Hassanien R., Ahmed M. (**2021**) A facile method for preparation and evaluation of the antimicrobial efficiency of various heterocycles containing thieno [2, 3-d] pyrimidine. *Synth. Commun.,* 51 (3), 398-409.

16 Ahmed M., Sayed M., Saber F. A., Hassanien R., El-Deana K. M. A., Tolba S. M. (**2022**) Synthesis, characterization, and antimicrobial activity of new thienopyrimidine derivatives. *Polycyclic Aromatic Compounds,* 42 (6), 3079-3088.

17 El-Deana K. M. A., Zaki M. R., Redwan M. S., Saber F. A., (**2017**) Synthesis, reactions and spectral characterization of novel thienopyrazole derivatives. *Eur. Chem. Bull.,* 6 (12), 550-553.

18 Zaki M. R., El-Deana K. M. A., Radwan M. S., Saber F. A., (**2019**) Efficient synthesis, reactions and spectral characterization of pyrazolo [4', 3': 4, 5] thieno [3, 2-d] pyrimidines and related heterocycles. *Heterocycl. Commun.,* 25 (1), 39-46.

19 Saber F.A., Z., Zaki M. R., El-Deana K. M. A., Radwan M. S., (**2020**) Synthesis, reactions, and spectral characterization of some new biologically active compounds derived from thieno [2, 3-c] pyrazole-5-carboxamide. *J. Heterocycl. Chem.,* 57 (1), 238-247.

20 Zaki M. R., El-Deana K. M. A., Radwan M. S., Saber F.A., (**2018**) A convenient synthesis, reactions and biological activity of some new 6h-pyrazolo [4', 3': 4, 5] thieno [3, 2-d][1, 2, 3] triazine compounds as antibacterial, anti-fungal and anti-inflammatory agents. *J. Braz. Chem. Soc.,* 29, 2482-2495.

21 Baranowski M., Dyksik M., Płochocka P., (**2022**) 2d metal halide perovskites: A new fascinating playground for exciton fine structure investigations. *Sci. Rad,* 1 (1), 3-25.

22 Klug T. M., Osherov A., Haghighirad A. A., Stranks D. S., Brown R. P., Bai S., Wang W. T. J., Dang X., Bulović V., Snaith J. H., Belcher M. A., (**2017**) Tailoring metal halide perovskites through metal substitution: Influence on photovoltaic and material properties. *Energy Environ. Sci,* 10 (1), 236-246.

23 Wu X. S., Weidong L., Qian Z., Xixia H., Dongsheng Q., Zewei (**2018**) Synthesis of lead-free csgei3 perovskite colloidal nanocrystals and electron beam-induced transformations. *Chem. Asian J.,* 13 (13), 1654-1659.

24 Volonakis G. H., Amir A. M., Rebecca L. S., Weng H. F., Marina R. W., Bernard J., Michael B. H., Laura M. S., Henry J., Feliciano G., (**2017**) Cs2inagcl6: A new lead-free halide double perovskite with direct band gap. *J. Phys. Chem. Lett.,* 8 (4), 772-778.

25 Gray M. B. M., Eric T W., Patrick M., (**2019**) Cs 2 agbibr 6− x cl x solid solutions–band gap engineering with halide double perovskites. *J. Mater. Chem. C,* 7 (31), 9686-9689.

26 Li Q. W., Yonggang P., Weicheng Y., Wenge Z., Bo T., Jiang Q., Zewei X., (**2017**) High-pressure band-gap engineering in lead-free $Cs_2AgBiBr_6$ double perovskite. *Angew. Chem. Int. Ed.,* 56 (50), 15969-15973.

27 Ogunniranye B. I., Oyewande E. O., Atsue T., Usikalu M., (**2021**) Influence of transition metal doping on the structural and electronic behaviour of quaternary double perovskite, cs2agincl6, using first-principles calculations. *IOP Conf. Ser.: Earth Environ. Sci. 655 012046.*

28 Razavi K. H., Edalati K., Wu J., Nakashima Y. Arita M., IkomaY., Sadakiyo M., Inagaki Y., Staykov A., Yamauchi M., Horita Z., Fuji M. (**2017**) High-pressure zinc oxide phase as visible-light-active photocatalyst with narrow band gap. *J. Mater. Chem.,* 5 (38), 20298-20303.

29 Bi P. Z., Shaoqing R., Junzhen C., Zhihao Z., Zhong C., Yong W., Jianqiu W., Shijie Z., Tao L., Jiayao F. (**2022**) A high-performance nonfused wide-bandgap acceptor for versatile photovoltaic applications. *Adv. Mater.,* 34 (5), 2108090.

30 Razumovskiy V. I., Lozovoi Y. A., Razumovskii M. I., (**2015**) First-principles-aided design of a new ni-base superalloy: Influence of transition metal alloying elements on grain boundary and bulk cohesion. *Acta Mater.,* 82, 369-377.

31 Li X., Muwei L., Hongbo W., Hongzhi X., Meng R., Hongpan W., Jing L., Jia L., Jiajia C., Wenxing J., (**2020**) Cation/anion exchange reactions toward the syntheses of upgraded nanostructures: Principles and applications. *Matter,* 2 (3), 554-586.

32 Mccall K. M. (**2019**), Synthesis, crystal growth, and optoelectronic characterization of inorganic halide perovskites as semiconductors for hard radiation detection. ProQuest no: 13807148, *ProQuest Dissertations Publishing,* United States.

33 Cai Y. X., Wei D., Hong C., Yan T., Krishnamoorthy W., Lydia H M., Nripan M., Subodh S., Matthew A., Mark G. (**2017**) Computational study of halide perovskite-derived a2bx6 inorganic compounds: Chemical trends in electronic structure and structural stability. *Chem. Mater.,* 29 (18), 7740-7749.

34 Ray A. D. T., Luca Z., Juliette I., Ivan M., Liberato A., Ahmed L. (**2022**) Light emission from low-dimensional pb-free perovskite-related metal halide nanocrystals. *Adv. Opt. Mater.*, 2202005.

35 Tang Y. T., Songzhi L., Ming G., Yanmei Z., Yingping L., Yongbing Z., Yixin F.(**2021**) All-inorganic lead-free metal halide perovskite quantum dots: Progress and prospects. *Chem comm,* 57 (61), 7465-7479.

36 Sohier T., Matteo M., Francesco C. (**2016**) Two-dimensional fröhlich interaction in transition-metal dichalcogenide monolayers: Theoretical modeling and first-principles calculations. *Phys. Rev. B.,* 94 (8), 085415.

37 Hammer B. H., Lars Bruno N., Jens K. (**1999**) Improved adsorption energetics within density-functional theory using revised perdew-burke-ernzerhof functionals. *Phys. Rev. B.,* 59 (11), 7413.

38 Adamo C., Vincenzo B., (**2002**) Physically motivated density functionals with improved performances: The modified perdew–burke–ernzerhof model. *Chem. Phys.,* 116 (14), 5933-5940.

39 Khein A. S., David J. U., Cyrus J. (**1995**) All-electron study of gradient corrections to the local-density functional in metallic systems. *Phys. Rev. B.,* 51 (7), 4105.

40 Tran F., Robert B., Peter S., Karlheinz L., (**2007**) Performance on molecules, surfaces, and solids of the wu-cohen gga exchange-correlation energy functional. *Phys. Rev. B.,* 75 (11), 115131.

41 Pedroza L. S. D. S., Antonio J., Klaus C., (**2009**) Gradient-dependent density functionals of the perdew-burke-ernzerhof type for atoms, molecules, and solids. *Phys. Rev. B.,* 79 (20), 201106.

42 Faizan M. B., Murtaza K., Ghulam H., Kulhari X., Neeraj A. A., Murefah M. K., Shah H. (**2021**) Electronic and optical properties of vacancy ordered double perovskites a2bx6 (a= rb, cs; b= sn, pd, pt; and x= cl, br, i): A first principles study. *Sci. Rep.,* 11 (1), 1-9.

43 Ahmed S. J., Abdul I., Syed Z. M., Hareem A., Simeon A., (**2021**) The first-principles prediction of two-dimensional indium-arsenide bilayers. *Mater. Sci. Semicond. Process,* 134, 106041.

44 Wiser N. (**1963**) Dielectric constant with local field effects included. *Phys. Rev. ,* 129 (1), 62.

45 Chaudhry A. R. H., Bakhtiar U. A., Shaari S., Laref A., (**2021**) Computational investigation of electronic and optical properties of spinal sulfides sc2xs4 (x= zn, mg and be) for photovoltaic and solar cell applications. *Mater. Sci. Semicond. Process,* 121, 105435.

46 Kumer A., and Chakma U. (**2021**) Developing the amazing photocatalyst of znag2gese4, znag2ge0. 93fe0. 07se4 and znag2ge0. 86fe0. 14se4 through the computational explorations by four dft functionals. *Heliyon,* 7 (7), e07467.

47 Howlader D. H., Sayed M., Chakma U. Kumer A., Mohammad J. I., Tawhidul M. Hossain T., Islam J., (**2021**) Structural geometry, electronic structure, thermo-electronic and optical properties of gacuo2 and gacu0. 94fe0. 06o2: A first principle approach of three dft functionals. *Mol Simul,* 47 (17), 1411-1422.

48 Chakma U., Kumer A., Al M., Hossain M., Alam M., Islam M., Shaikh R. M., Jony I. J., Islam J., (**2022**) Investigation of electronic structure, optical properties, map of electrostatic potential, and toxicity of Hfo_2, $Hf_{0.88}si_{0.12}o_2$, $Hf_{0.88}Ge_{0.12}o_2$ and $Hf_{0.88}Sn_{0.12}O_2$ by computational and virtual screening. *J. Comput. Electron.*, 1-16.

49 Rahman M. A. Chakma U., Kumer A. Rahman, M. R., Mahbubul M. M., (**2023**) Uridine-derived 4-aminophenyl 1-thioglucosides: Dft optimized fmo, adme, and antiviral activities study, *Biointerface Res. Appl. Chem.*, 13 (1), 1-15.

50 Kobir M. E., Asif A., Roni M. A. H. Chakma U., Amin M. R., Chandro A., Kumer A., (**2022**) Anti-lung cancer drug discovery approaches by polysaccharides: An in silico study, quantum calculation and molecular dynamics study. *J. Biomol. Struct. Dyn.,* 1-17.

51 Chakma U. K., Ajoy Hossain, Tomal Hossain, Md Sayed Alam, Md Monsur Islam, Md Shariful Shaikh, Rubel Islam, Jahedul (**2022**) Investigation of electronic structure, optical properties, molecular electrostatic potential maps (epm) and aquatic toxicity of hfo2, hf0. 88si0. 12o2, hf0. 88ge0. 12o2 and hf0. $88sn_{0.12}o_2$ by computational methods, *researchsquare, 1-18.*

52 Kumer A. Chakma U. Alam M. M., Chakma P., Islam M. S., Khandaker N. Z., Hossain T. Chowdury A. N. (**2022**) Structural, electronic, and opto-electronic properties for bivs4 photocatalyst effort on wastewater treatment with comparison a standard photocatalyst bivo4 through the first principles. *ECS Transactions,* 107 (1), 12109.

53 Mahmud M. A., Kumer A. Chakma U., Howlader D. Hoque K. A. Chowdury A. N. (**2022**) Fabrication of computationally designed cathode material for a high-performance na-ion battery. *ECS Transactions,* 107 (1), 15681.

54 Hoque K. A., Kumer A., Chakma U. Chowdury A. N. (**2022**) Facile synthesis of computationally designed mgal2o4/ceo2/cu2o and mgal2o4/ceo2/ag2o smart heterojunction photocatalysts for aqueous organic pollutants degradation. *ECS Transactions,* 107 (1), 13785.

55 Ali M. I., Mohammad J., Kumer A., Hossain M., Chakma U. Howlader D., Islam M., Hossain, T. (**2021**) Investigation of structural, electronic and optical properties of na 2 inagcl 6, k 2 inagcl 6, and rb 2 inagcl 6 lead-free halide double perovskites regarding with cs 2 inagcl 6 perovskites cell and a comparative study by dft functionals. *Mater. Res.,* 24.

56 Al M. A., Habib A. M., Chakma U., Sikder M., Kumer A., (**2021**) Structural, electronic, optical properties and molecular dynamics study of wo3 w0. 97ag0. 03o3 and w0. 94ag0. 06o3 photocatalyst by the first principle of dft study. *Egypt. J. Chem.,* 64 (9), 5117-5126.

57 Hasan M. M., Kumer A., Chakma U., Tawhidul I. M. (**2021**) Structural, optical and electronic properties of znag 2 gete 4 and znag 2 ge 0.93 fe 0.07 te 4 photocatalyst: A first principle approach. *Mol. Simulat,* 47, 1-13.

58 Ali M. I., Rafid M., Jeetu M., Roy R. R, Chakma U, (**2021**) The computational screening of structural, electronic, and optical properties for sic, si0. 94sn0. 06c, and si0. 88sn0. 12c lead-free photovoltaic inverters using dft functional of first principle approach. *Eurasian Chem. Commun. ,* 3 (5), 327-338.

59 Sikder M. M. Chakma U., Kumer A. Islam M. J., Habib A. Alam M. M. (**2021**) The exploration of structural, electronic and optical properties for mos2 and mo0. 95w0. 05s2 photocatalyst effort on wastewater treatment using dft functional of first principle approach. *Appl. J. Environ. Eng,* 7 (1), 7-1 (2021) 2103-2113.

60 Hossain T. H., Ali M. H., Chakma U. Kumer A. Islam M. J. (**2021**) Investigation of optoelectronics, thermoelectric, structural and photovoltaic properties of ch3nh3snbr3 lead-free organic perovskites. *Chem. Methodol.,* 5 (3), 259-270.

61 Islam M. T., Kumer A., Chakma U. Howlader D. (**2021**) A computational investigation of electronic structure and optical properties of alcuo2 and alcu0. 96fe0. 04o2: A first principle approach. *Orbital: J. Chem.,* 58-64.

62 Chakma K. B. Kumer A. Chakma U. Howlader D. Islam M. T., (**2020**) A theoretical investigation for electronics structure of mg (bio2) 2 semiconductor using first principle approach. *Int J New Chem,* 7 (3), 247-255.

63 Chakma U. Kumer A., Chakma K. B., Islam M. T. Howlader D. Mohamed R. M.,(**2020**) Electronics structure and optical properties of srpbo3 and srpb0. 94fe0. 06o3: A first principle approach. *Eurasian Chem Commun,* 2 (5), 573-580.

64 Islam M. T., Kumer A., Howlader D, Chakma K. B. Chakma U. (**2020**) Electronics structure and optical properties of mg (bio2) 4 and mg (bi0. 91ge0. 083o2) 4: A first principle approach. *Comput. Theor. Chem.,* 4 (1), 24-31.

65 Hasan M. M. Kumer A., Chakma U., (**2020**) Theoretical investigation of doping effect of fe for snwo4 in electronic structure and optical properties: Dft based first principle study. *Adv. J. Chem. A ,* 3 (5), 639-644.

66 Chakma U. Kumer A. Chakma K. B., Islam M. T. Howlader D., (**2020**) Electronics structure and optical properties of ag2bio3,(ag2) 0.88 fe0. 12bio3: A first principle approach. *Adv. J. Chem. A ,* 3 (4), 542-550.

67 Islam J. Kumer A. Chakma U. Alam M., Biswas S., Ahmad Z., Islam M., Jony M. I. J., Ahmed M. B. Investigation of structural, electronic, and optical properties of srtio3 and srti0. 94ag0. 06o3 quantum dots based semiconductor using first principle approach. *Adv. J. Chem. A,* 5 (2), 164-174.

© 2023 by the authors; licensee Growing Science, Canada. This is an open access article distributed under the terms and conditions of the Creative Commons Attribution (CC-BY) license (http://creativecommons.org/licenses/by/4.0/).